

Dry Electrode-Based Fully Isolated EEG/fNIRS Hybrid Brain-Monitoring System

Seungchan Lee , Younghak Shin , *Member, IEEE*, Anil Kumar , *Member, IEEE*, Minhee Kim, and Heung-No Lee , *Senior Member, IEEE*

Abstract—A portable hybrid brain monitoring system is proposed to perform simultaneous 16-channel electroencephalogram (EEG) and 8-channel functional near-infrared spectroscopy (fNIRS) measurements. Architecture-optimized analog frontend integrated circuits (Texas Instruments ADS1299 and ADS8688A) were used to simultaneously achieve 24-bit EEG resolution and reliable latency-less ($<0.85 \mu\text{s}$) bio-optical measurements. Suppression of the noise and crosstalk generated by the digital circuit components and flashing NIR light sources was maximized through linear regulator-based fully isolated circuit design. Gel-less EEG measurements were enabled by using spring-loaded dry electrodes. Several evaluations were carried out by conducting an EEG phantom test and an arterial occlusion experiment. An alpha rhythm detection test (eye-closing task) and a mental arithmetic experiment (cumulative subtraction task) were conducted to determine whether the system is applicable to human subject studies. The evaluation results show that the proposed system is sufficiently capable of detecting microvoltage EEG signals and hemodynamic responses. The results of the studies on human subjects enabled us to verify that the proposed system is able to detect task-related EEG spectral features such as eye-closed event-related synchronization and mental-arithmetic event-related desynchronization in the alpha and beta rhythm ranges. An analysis of the fNIRS measurements with an arithmetic operation task also revealed a decreasing trend in oxyhemoglobin concentration.

Index Terms—Electroencephalogram (EEG), functional near-infrared spectroscopy (fNIRS), hybrid brain-computer interface, multimodal analysis, portable instrument, simultaneous measurement.

Manuscript received April 12, 2018; revised July 19, 2018; accepted August 10, 2018. Date of publication August 27, 2018; date of current version March 19, 2019. This work was supported by the National Research Foundation of Korea (NRF) funded by the Korean government (MISP) under Grants [NRF-2018R1A2A1A19018665] and [NRF-2015A2A1A05001826], and by the Brain Research Program through the NRF funded by the Ministry of Science, ICT & Future Planning under Grant [NRF-2016M3C7A1905475]. (*Corresponding author: Heung-No Lee.*)

S. Lee, A. Kumar and H.-N. Lee are with the Department of Electrical Engineering and Computer Science, Gwangju Institute of Science and Technology, Gwangju 61005, South Korea (e-mail: future-max7@gmail.com, heungno@gist.ac.kr).

Y. Shin is with the Department of Electronic Systems, Norwegian University of Science and Technology.

M. Kim is with the Department of Biomedical Science and Engineering, Institute of Integrated Technology, Gwangju Institute of Science and Technology.

Digital Object Identifier 10.1109/TBME.2018.2866550

I. INTRODUCTION

THE brain-computer interface (BCI) [1], [2] was originally developed to assist severely disabled people who cannot control their peripheral nerves and muscles, due to neurological and neuromuscular disorders such as amyotrophic lateral sclerosis, brainstem strokes, and spinal cord injuries. This technology is now advancing to provide a new communication channel that facilitates human-machine interaction. Presently, a number of new techniques based on wearable devices and the Internet of Things (IoT) are being applied to BCIs related to the fields of healthcare, telemedicine, and clinical care [3]. Current BCI technology, however, faces several challenges, such as its limited number of controllable functional-brain signals [4], the need for recalibration of the signal processing algorithms, and uncontrollability for a non-negligible proportion of the users, referred to as “BCI-illiteracy” [5].

Multimodal analysis of brain activities—the so-called hybrid BCI [6], which can be implemented by simultaneously acquiring and analyzing two or more brain signals, has been proposed as an alternative BCI technique capable of overcoming the above challenges. Two or more complementary neurological signals can be combined and shared to maximize the amount of exploitable information, thereby enhancing the robustness of control accuracy in real-world applications.

Hybrid BCI systems could be established by the fusion of two or more modalities amongst various brain imaging techniques, such as electroencephalogram (EEG), magnetoencephalogram (MEG), functional magnetic resonance imaging (fMRI), and functional near-infrared spectroscopy (fNIRS). Among these modalities, the disadvantages of MEG- and fMRI-based techniques is the need to install the machines in confined areas and the fact that they can only be used for short runtimes because of their high cost, large size, and the need for expert operators [7]. Contrary to this, EEG- and fNIRS-based brain-monitoring systems are electromechanically simple, making them easy to design for lightweight, compact and low-cost systems. EEG/fNIRS-combined hybrid systems could easily be built as portable or wearable devices and utilized in more dynamic applications, such as driver drowsiness detection [8] and seizure monitoring in epileptic patients [9].

An EEG is the electrical potential produced by the sum of the synchronous activation from the dendritic branches of a large number of neurons. Because EEG recording can be achieved noninvasively through the electrodes placed on the scalp and its

time resolution is relatively high in the millisecond range, it is widely used as an electrophysiological recording modality [2]. On the other hand, fNIRS measures the changes in the local concentration of oxygenated and deoxygenated hemoglobin in the cerebral cortex region by utilizing low-energy optical radiation from light sources of two different wavelengths in the near-infrared range (700–1000 nm). Although this technique demonstrates a slower response compared to EEG, it enables an investigation of metabolic and microcirculatory neuronal activation regardless of the electrically synchronized activation of neurons [10]. The simultaneous acquisition of EEG and fNIRS measurements could provide more comprehensive neurodynamic information regarding the accessible neuronal metabolism and neuroelectric activities. As such, several researchers have recently developed EEG–fNIRS hybrid systems for use in various applications [11].

A review of the available literature related to hybrid BCI systems indicates that a combination of individual EEG and fNIRS systems has been used in various experimental accomplishments regarding motor imageries [12]–[16], visual and auditory stimulations [17] and mental workloads [18], [19]. In such a setup, fully synchronized operation of the entire system is difficult, because each individual system contains its own controller that is operated at a predefined clock speed. Therefore, the measurements acquired from two systems may not be completely synchronized in the absence of a precise simultaneous control mechanism. Attempts to address this concern have resulted in the design of customized EEG–fNIRS hybrid acquisition instruments.

One of the first attempts to this end has been started with the design of a probe for simultaneous measurements of EEG and fNIRS data [20]. Lareau *et al.* [21] and Sawan *et al.* [22] have proposed a similar hybrid system that was capable of acquiring multi-channel EEG and fNIRS measurements. However, it was difficult to use it as an out-of-lab device because of its large size ($16 \times 13 \times 8.2 \text{ cm}^3$). In 2013, a field-programmable gate array (FPGA) and an EEG application-specific integrated circuit (ASIC) based compact, and advanced bimodal acquisition system was developed by Safaie *et al.* [23]. Recently, Luhmann *et al.* [24] developed a miniaturized modular hybrid system, wherein one module was capable of simultaneously monitoring four channels of bio-electrical and bio-optical measurements. However, these reported studies still have several limitations related to practical usability in daily-life monitoring. The conductive gel of conventional wet electrodes leads to user irritation and easily degrades the signal quality as it becomes dry, making long-term monitoring difficult. Efficient suppression of the crosstalk and noise characteristics in a mixed-signal system is another key challenge in designing a hybrid instrument.

This paper proposes a dry electrode-based portable hybrid brain monitoring (HBM) system that provides simultaneous monitoring of fully synchronized 16-channel EEG and 8-channel fNIRS. Aiming at a use of out-of-lab and clinical applications, the performance and availability of the instrument have been improved by integrating the following advanced features with the proposed system:

- 1) Dry electrode-based gel-less EEG acquisition [25]–[27] for easy to put on, non-degraded EEG quality, and significant reduction in wearing time to less than 10 minutes (refer to Section II-C);
- 2) Architecture-optimized frontend design for sufficient resolution EEG and timing-secured errorless bio-optical measurement, i.e., delta-sigma (Δ - Σ) architecture ADC-based 24-bit EEG resolution and successive approximation register (SAR) architecture ADC-based latency-less ($<0.85 \mu\text{s}$) bio-optical measurements (refer to Section II-A);
- 3) Linear regulator-based fully-isolated circuit design for maximization of noise and crosstalk suppression (refer to Section II-B);
- 4) Customizable EEG electrode-positioning structure (named as EEGCAP) to meet various experimental scenarios (refer to Section III-B-1)).

Several evaluation tests were performed to verify the hybrid data acquisition performance. The acquisition of EEG measurements using the dry electrodes was evaluated by performing an EEG phantom test. An arterial occlusion experiment was performed to verify the hemodynamic responses of the fNIRS measurements. Finally, human subject studies including an alpha rhythm detection test and an experiment to assess mental arithmetic operation were performed to verify the practical capabilities for EEG and fNIRS feature measurements.

The remainder of the paper is organized as follows: Section II and III provide detailed descriptions of the design methods and the implementation of the proposed system, respectively. The evaluation of the EEG/fNIRS measurements and human subject studies, including an alpha rhythm detection test and a mental arithmetic operation experiment, are presented in Section IV. Section V summarizes several results, including system implementation, acquisition capability evaluation, and offline analysis of human subject studies. The contributions of this study are discussed in Chapter VI in comparison with previous studies. Finally, concluding remarks with a summary of the system design and experimental results are given in Section VII.

II. SYSTEM DESIGN

This section describes the key design methods for implementing the proposed HBM system, namely *architecture-optimized frontend design*, *linear regulator-based fully-isolated circuit design*, and *dry electrode-based gel-less EEG acquisition*.

A. Architecture-Optimized Frontend Design

Physiological signals, such as EEG and fNIRS, possess small amplitudes and are highly susceptible to various types of noise. For this reason, the use of complicated signal-conditioning circuits becomes necessary to achieve high-precision measurements. State-of-the-art integrated analog frontend (AFE) integrated circuits (ICs) combined with high-resolution analog-to-digital converters (ADCs), signal-conditioning circuits, and associated built-in circuits and their design benefits were reported [28]. The integrated functions of these ICs assist to reduce the number of discrete components required in the design of a data

acquisition system, enabling miniaturized and low-cost designs with reliable performance.

The proposed design employs the ADS1299 AFE IC (Texas Instruments, USA) [29] for EEG measurements. It was integrated with 8-channel, 24-bit resolution Δ - Σ ADCs, programmable gain amplifiers (PGAs), and other built-in peripherals. A sufficiently small step size of the least significant bit (LSB) ($0.022 \mu\text{V}$ at a 24 PGA gain) and low peak-to-peak noise performance ($0.98 \mu\text{V}$ at a 250-SPS sampling rate and a 24 PGA gain) enables precise detection of EEG signals in the μV range. The integrated 8-channel ADCs allow simultaneous sampling of multiple input measurements, thus no sampling skew and glitch noise exist in the converted data without the need for sample-and-hold circuits.

Although the ADS1299 was used for EEG measurements in previous studies [24], this is the first time the ADS8688A (Texas Instruments, USA) [30] was used for the acquisition of bio-optical measurements. This device is a 16-bit successive SAR ADC-based AFE integrated with numerous built-in functions such as 8-channel input multiplexer, PGAs, and second-order low-pass filters.

Compared to the Δ - Σ architecture employed in ADS1299, the SAR ADC architecture [31] can provide the precise delay-less measurement required for bio-optical acquisition. The delta sigma architecture is advantageous for acquiring high-resolution measurements exceeding 20 bits; however, its operating mechanism requires the use of a digital decimation filter for noise-shaped representation of oversampled data, thereby resulting in conversion latency known as the settling time [32]. This latency represents the delay between the beginning of the input signal conversion and the end time at which fully settled output data are available. In the case of the ADS1299, this latency reaches 16 ms at a sampling rate of 250 SPS. Unlike delta-sigma ADCs, the SAR ADC architecture does not require the conversion latency because it repeatedly performs a zero-latency task, which compares the reference voltage and input measurements through a sample-and-hold circuit, a comparator, and a DAC. This zero-latency feature, which produces digitized data within $0.85 \mu\text{s}$ in case of the ADS8688A, leads to reliable delay-less measurement. Because the bio-optical measurement requires on-time acquisition within predefined timing bins (4 ms) when the NIR light source is in an active state, this delay-less characteristic is essential for accurate acquisition of bio-optical measurements. Therefore, the ADS8688A, instead of the ADS1299, which is Δ - Σ architecture ADC-based AFE IC, is employed for the bio-optical measurement.

B. Linear Regulator-Based Fully-Isolated Circuit Design

In mixed-signal systems in which analog and digital components are integrated into a single circuit, the crosstalk noise generated in digital circuits could be coupled to neighboring analog circuits via stray capacitances [33]. In the proposed HBM system, a periodical switching operation of the NIR light source is necessary to acquire bio-optical measurements. The oscillating noise in the digital circuits is unavoidable because of the instantaneously high current flow in the driving circuit of the

light source. Without careful consideration of the crosstalk, this noise may appear on the analog circuits associated with the AFE ICs and can easily distort the small EEG and bio-optical amplitudes.

The crosstalk rejection capability was maximized by implementing a fully isolated circuit design technique, such as a circuit design with separate ground planes and an isolated digital interface, in the power and control circuits of the proposed system. The design of the power supply circuit included the use of a dedicated lithium-polymer battery and an isolated DC-DC converter (DCP020509, Texas Instruments, USA) to separate the ground for the data acquisition circuits and the digital control circuit. This design results in a total of three completely separated ground planes. Since independent return current paths are created on each ground plane and these paths are completely isolated from each other, the switching noise generated in the control circuit cannot reach the data acquisition areas. Therefore, the EEG and fNIRS acquisition circuits are able to maintain flat and stable ground potentials. Two digital isolators (Silicon Labs Si8662) are also used for the isolated interface of the EEG and fNIRS acquisition circuits. Many advanced features, such as high data throughput, low propagation delay, and noise robustness of the isolator IC serve to provide a reliable and uncoupled data path in the digital interface.

The linear regulator-based power supply circuits were carefully designed by using a number of decoupling capacitors and ferrite beads to provide low-noise DC power to the data acquisition circuits. The linear regulators provide several advantages compared to DC-DC converters, such as highly regulated output voltage, low noise spectral density, and a high power supply rejection ratio (PSRR), thereby making them ideally suited for noise-sensitive applications. In addition to these low-noise power supply circuits, an optimized printed-circuit-board (PCB) layout and advanced circuit-design techniques, such as grounding, signal routing, and decoupling [34], were applied to maintain stable and regulated DC voltages and build a low-impedance return current path.

C. Dry Electrode-Based Gel-Less EEG Acquisition

Conventionally, disc-shaped Ag/AgCl electrodes have been employed in EEG measurements. These electrodes require the use of conductive gels and hair preparation during installation in order to reduce the electrical impedance to an acceptable level. These procedures are time consuming and cause irritation in most subjects, because conductive gels are sticky. Moreover, these electrodes are not suitable for long-term and ambulatory applications, because conductive gels dry over time and their adhesion is easily lost during motional vibrations. Therefore, the signal quality of the wet electrodes may be continuously degraded in ongoing experiments, thus the use of wet electrodes is to be limited in experiments requiring more than 30 minutes. To overcome these problems, dry electrodes, which do not require conductive gels, are used in the proposed system. These electrodes comprise spring-loaded probes that maintain a constant pressure on the surface of the uneven scalp regardless of its movement. Consequently, these electrodes are capable of more

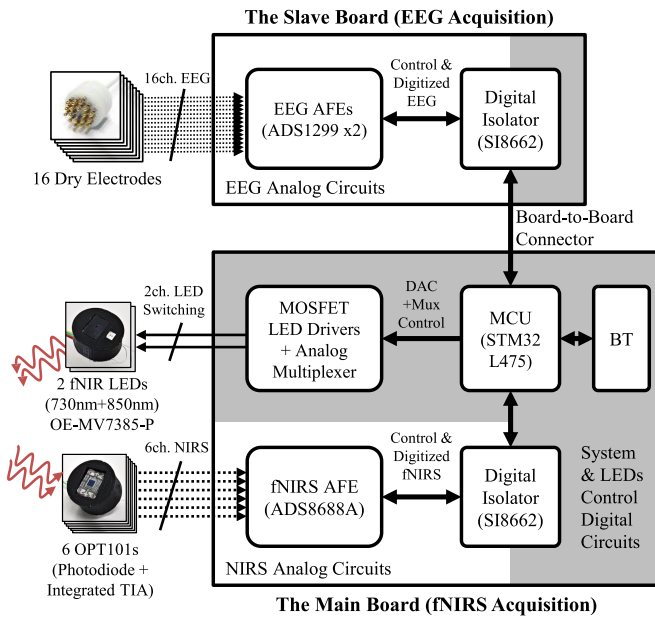


Fig. 1. Simplified schematic of the proposed HBM system. Solid and dotted arrows indicate the flow of digital logic signals and analog measurements, respectively. Likewise, the shaded and transparent regions indicate the digital and analog circuits, respectively. The boundary between the analog and digital circuits is isolated by a digital isolator and DC-DC converter. The dedicated EEG acquisition circuits is also isolated from the main board circuits.

stable EEG measurements even in out-of-lab environments. The dry-electrode structure is described in detail in Section III-B-1).

III. IMPLEMENTATION

A. Instrumentation

1) Data Acquisition Circuit: Fig. 1 depicts a schematic of the proposed system excluding the power supply circuits. The system comprises two boards—the main board and slave board. The main board is capable of performing 8-channel bio-optical measurements, and 4-channel dual-wavelength LED emissions. The slave board was designed to perform 16-channel EEG measurements. The two boards were connected using the Molex board-to-board connector, and all components were controlled by the STM32L475 low-power microcontroller (STMicroelectronics, USA) installed on the main board.

The following procedure was used to perform bio-optical measurements on the main board. Common-mode electromagnetic and radio-frequency interference noise is first filtered out from raw bio-optical measurements using a simple RC low-pass filter in the input stage. Inside the embedded ADS8688A AFE IC, the acquired bio-optical signal is amplified by the integrated PGA to pre-programmed input ranges (± 0.64 V) and subsequently filtered by an anti-aliasing low-pass filter with a 15-kHz cutoff frequency. Because the actual sampling rate of the bio-optical measurement reaches 20 kHz to obtain an averaged measurement from quick repeated samples, the built-in anti-aliasing filter is required for aliasing rejection. The filtered signal is then fed to the ADC driver and multiplexer circuits, and is finally sampled by a 16-bit SAR ADC. According to this

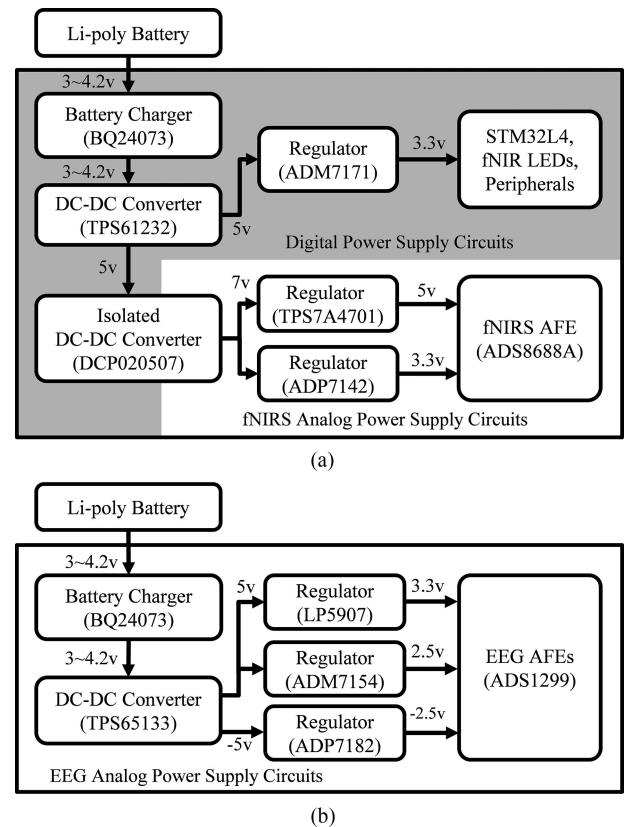


Fig. 2. Schematics of power-supply circuit for (a) main board, and (b) slave board. Two lithium-polymer batteries supply power to the main board and the slave board, respectively. In the main board, the isolated DC-DC converter separates the ground planes for the main control circuit (shaded digital power supply section) and the isolated NIRS acquisition circuit (fNIRS analog power supply section).

procedure, 8-channel bio-optical data can be finally obtained at a 5-SPS sampling rate.

The following procedure was also used to perform EEG measurements on the slave board. The EEG measurements acquired by the dry electrodes are filtered by the onboard input filter stage. X2Y type capacitors [35] were employed in this filter stage to facilitate higher attenuation of electromagnetic and radio-frequency noise, while reducing onboard space requirements. Inside the ADS1299 AFE IC, the filtered EEG measurements are amplified by a built-in low noise PGA with a 24 gain setting and digitized by a dedicated ADC for each channel over every sampling period (4 ms). The sampled EEG data are then transmitted to the microcontroller (MCU) via an SPI bus. With two ADS1299s in a daisy-chained configuration that allows multiple ICs to be controlled simultaneously using a single shared bus, 16-channel EEG measurements can be obtained at a 250-SPS sampling rate.

2) Power Supply Circuit: Fig. 2 depicts a schematic of the power-supply circuits of the proposed HBM system. The proposed system is powered by two lithium-polymer batteries—one each for the main and slave boards—which can be charged via the onboard battery management IC (Texas Instruments BQ24073) through a USB port. As the battery

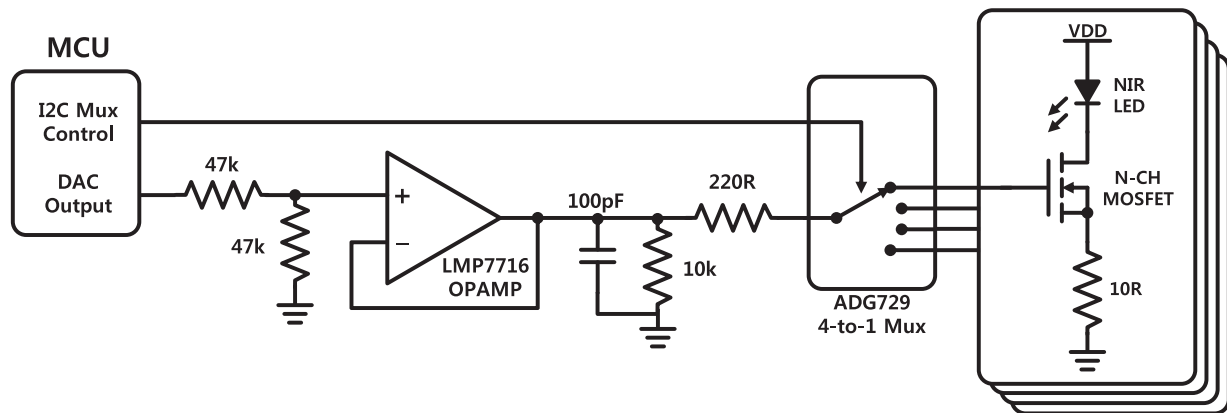


Fig. 3. Schematic of the MOSFET-based NIR LED driving circuit employed in the proposed HBM system. This circuit was combined with a DAC, analog multiplexer, and OPAMP-based buffering circuit to flexibly control the emission intensity of the four LEDs. By implementing two copies of this circuit, the proposed system can control up to eight LED emissions.

voltage decreases over time, boost and dual-output DC–DC converters (Texas Instruments TPS61232, TPS65133) are used to stabilize these output voltages. An isolated DC–DC converter (Texas Instruments DCP020507) is employed to supply fully isolated power for the fNIRS acquisition circuits on the main board. In the final stage of the power-supply circuits, low-noise DC voltage is lastly delivered to the AFE ICs, MCU, and other peripherals through six low-noise linear regulators (Analog Devices—ADM7154, ADP7182, ADP 7142, and ADM7171; Texas Instruments—TPS7A4701 and LP5907).

3) MOSFET-Based LED Driving Circuit: Fig. 3 illustrates the schematic of the MOSFET-based LED driving circuit. Because the number of NIR light sources required may vary depending on the configuration of the probe set layout and the experimental paradigm, a programmable control function for multi-channel emission is required for the LED driving circuitry. A calibration function for radiant intensity is also necessary because the NIR LED may exhibit radiant power mismatch even for the same current consumption. Thus, a programmable LED driving circuit was designed to flexibly control the radiant intensity of multi-channel NIR LEDs by combining a digital-to-analog converter (DAC), an analog multiplexer and MOSFET drivers. In operation, the MCU regulates the gate voltage of the MOSFET driver by controlling the output voltage of the built-in digital-to-analog converter (DAC) of the MCU. The regulated gate voltage is buffered with an OPAMP and then fed to the analog multiplexer (Analog Device ADG729) for controlling multi-LED emissions. The multiplexed gate voltage is lastly supplied to the N-channel MOSFET driver to modulate the LED current flow. This design provides flexibility to control as many as eight NIR LED emissions with fine-tuned radiant intensity in the proposed system. In the human subject studies described in this paper, the radiant intensity for all NIR LEDs was manually adjusted to 10 mW using an optical power meter and DAC output voltage control.

B. Sensors

Customized sensor units were designed for the EEG and bio-optical measurements to enhance the usability and re-

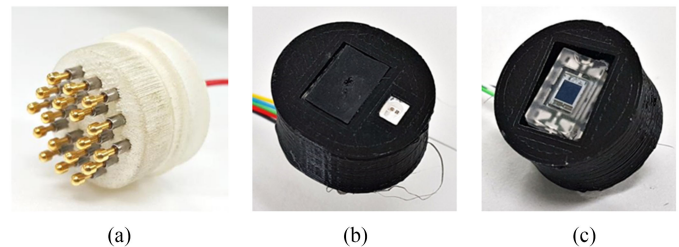


Fig. 4. (a) Dry electrode for EEG measurement, (b) dual wavelength LED-based NIR light source unit, and (c) silicon photodiode-based NIR detector unit for bio-optical measurement.

configurability of the proposed system. The sensor units comprise 16-channel dry electrodes, 2-channel NIR LEDs, and 6-channel photodiodes.

1) Spring-Loaded Dry Electrode and Customizable EEGCAP: The Fig. 4(a) depicts a prototype of the dry electrode for the EEG measurements, which comprises spring-loaded probes, a PCB, and a housing. The electrode unit, which is designed to remain in contact with the subject's scalp, acquires EEG potentials via the 18 spring-loaded probes (Leeno Industrial Inc., SK100R). Each probe comprises four components—the (1) plunger, (2) barrel, (3) spring, and (4) probe receptacles. The plunger is combined with a barrel and spring to constitute the spring-loaded structure. Each spring can withstand up to 54 g of pressure in its maximally compressed state. This enables each probe to maintain a suitable contact pressure on the uneven surface of the scalp. In terms of electrical specifications, the resistance of each probe is less than 50 mΩ, which is sufficiently low for conducting bioelectrical measurements. All probes are electrically connected to each other via the PCB embedded in the electrode housing and are thereby linked to a single electrode wire. The entire electrode assembly is enclosed by the 3D-printed plastic housing.

A helmet-like bracket (named the EEGCAP) was designed using flexible rubber materials to hold the dry electrodes in position in accordance with 10–20 systems. The mesh-type EEGCAP structure was equipped with as many as 58 holes to allow electrodes to be positioned on the scalp. Each electrode was

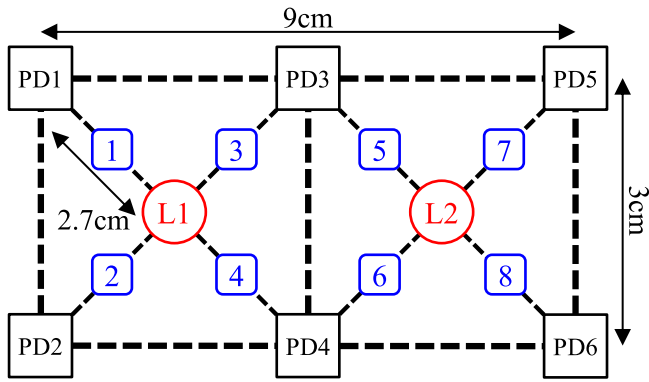


Fig. 5. Installation layout of NIR LEDs (L1 and L2) and photodiodes (PD1–PD6) for acquisition of the bio-optical measurements. To investigate hemodynamic changes at the frontal lobes, the light source and detector units are attached using a transparent double-sided tape. This layout produces 8-channel hemodynamic responses from the 1-to-8 bio-optical channels marked in blue color.

firmly engaged in the hole via an interlocking frame structure, and able to continuously push against the subject's scalp to maintain a constant pressure. This customizable structure could make a number of configuration choices available in terms of the electrode-positioning layout depending on the experimental paradigm.

2) NIR Light Source and Detector Units: Dual wavelength (730 and 850 nm) AlGaAs LEDs (Opto ENG OE-MV7385-P) were used for the NIR light source unit depicted in Fig. 4(b). Two LEDs packaged in a miniaturized plastic leaded chip carrier (PLCC) were soldered onto a light source PCB and covered by 3D printed materials. The spectral spread of the emitted radiation ($\Delta\lambda = 30\text{--}40$ nm) was broader compared to that of monochromatic laser diodes ($\Delta\lambda \approx 1$ nm). However, the incoherent and un-collimated characteristics of the LED light source achieve sufficient tissue penetration to enable the investigation of local hemodynamic changes. Owing to its suppressed heating and low risk of retinal damage, it can be used in direct contact with the human scalp [36].

The NIR detector unit depicted in Fig. 4(c) was based on a silicon photodiode device (Texas Instruments OPT101) integrated with an on-chip trans-impedance amplifier. Because the device exhibits high spectral sensitivity in the infrared spectrum (>0.5 A/W in the 730–850 nm wavelength), it is optimized for use in NIR detection applications. Owing to the built-in trans-impedance amplifier circuitry composed of an operational amplifier and an internal feedback network, the photodiodes provide direct voltage output with a sufficiently wide bandwidth (14 kHz) which is linearly proportional to the detected light intensity. The photodiode is soldered onto a detector PCB along with decoupling capacitors, and housed inside a 3D-printed-casing.

Fig. 5 illustrates the positioning layout for NIR LEDs and photodiodes for placement on the subject's forehead. The layout configuration occupies a $9\text{ cm} \times 3\text{ cm}$ area with two NIR LEDs and six photodiodes, and the distance between the light source and the detector unit was set at 2.7 cm. In operations using this layout, the NIR LEDs flicker alternately in accordance with the pre-programmed LED switching sequence and only the

photodiodes surrounding the turned-on LED are instantaneously activated. Each hemodynamic response is measured in the area between the pair of light sources and the detector unit and this area is defined as a bio-optical channel. To achieve the maximum number of bio-optical channels in the restricted forehead space, measurements for bio-optical channels 3 through 6 located between NIR LEDs L1 and L2 are all required. By exploiting a TDM-based channel-sharing scheme where one photodiode can provide multiple independent measurements in non-overlapped timing periods, the four independent measurements for these centrally located bio-optical channels can be provided from photodiodes PD3 and PD4; i.e., photodiode PD3 can provide measurements for the 3rd and 5th bio-optical channels and photodiode PD4 can provide measurements for the 4th and 6th optical channels in the same manner. Therefore, this channel sharing operation enables the proposed sensor layout to acquire 8-channel bio-optical measurements with only six photodiodes.

C. System Operation and Hybrid Data Acquisition

The ADC basically converts analog input signals into digitized signals with consistent intervals based on an internal or external reference clock. However, the clock may have its own tolerance and frequency drift characteristics. In heterogeneous data-acquisition systems employing two or more ADCs to produce a fully synchronized data stream, the clock tolerance of individual ADCs makes accurate synchronization difficult to achieve. This problem can be solved by using a reference system clock to which all ADCs could be universally referred.

Complete synchronization is achieved between the EEG and bio-optical measurements by using the data-ready signals (referred to as DRDY in the datasheet) generated by the ADS1299 AFE IC as the reference system clock. The DRDY signal represents the transition of a falling edge when the digitized EEG data stream becomes valid. It, therefore, generates a pulse signal of the same period as the sampling rate of EEG acquisition. By synchronizing the emission control of NIR LEDs and data acquisition of ADS8688A with the DRDY pulse cycle, the complete synchronization between EEG and bio-optical measurements can be preserved regardless of the occurrence of small timing errors in the reference clock of each AFE.

Fig. 6 depicts a single period of simultaneous EEG and bio-optical acquisition captured from the logic analyzer screen. Once ADS1299 begins to acquire EEG measurements at a pre-programmed sampling rate (250 SPS), the DRDY pulses begin to be generated with the same sampling period (4 ms) as EEG data generation. In accordance with the generation of the DRDY pulse, NIR radiation of dual wavelengths (730 and 850 nm) is alternately switched in the order—L1 (730 nm)—L2 (730 nm)—L1 (850 nm)—L2 (850 nm)—over the course of 50 EEG acquisition cycles (200 ms). Each time the NIR LED is turned on by the multiplexer switching, the radiation lasts for 4 ms, during which time the ADS8688A acquires NIR light intensities from the set of activated photodiodes surrounding the turned-on LED; i.e., when the L1–730 nm or L1–850 nm states are active, measurements from the photodiodes PD1–PD4 are sampled. This also applies to the two L2 states and sampling of photodiodes PD3–PD6. To

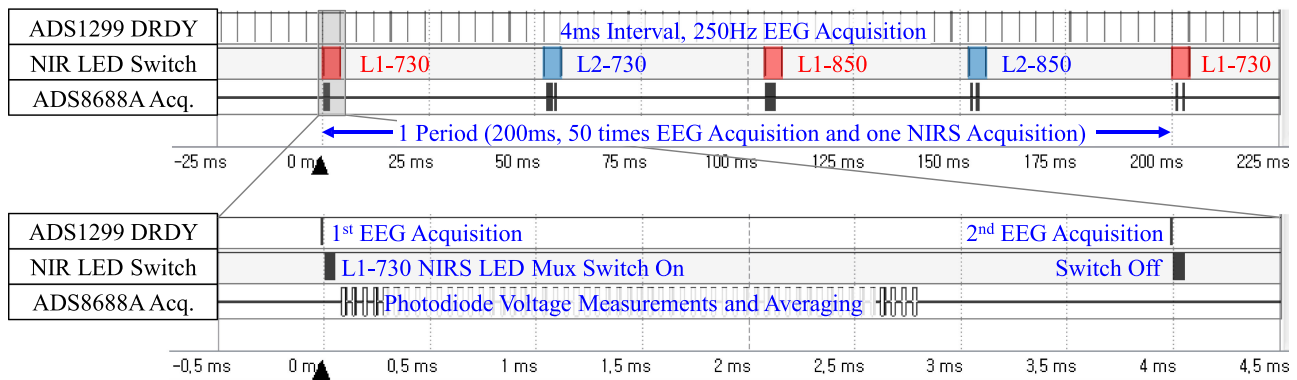


Fig. 6. Logic analyzer view of one period of simultaneous EEG and fNIRS acquisition and magnified view of the upper gray region (-0.5 – 4.5 ms). According to the DRDY pulse generated by the ADS1299, 16-channel EEG measurements are acquired, and the NIR light sources L1 and L2 are alternately activated for 4 ms. During NIR irradiation for 4 ms, each of the 4-channel photodiodes surrounding the light source measured the light intensity 14 times and averaged it. A total of 16-channel of bio-optical measurements are obtained over a 200-ms period, which is converted into 8-channels of fNIRS data during the fNIRS decoding process.

obtain stable measurements with minimized background noise, the light intensity measurement of each bio-optical channel is repeatedly acquired 14 times with a $50\text{-}\mu\text{s}$ interval and subsequently averaged. During the 4-ms period of LED radiation, a total of 56 optical measurements are then sequentially obtained within 2.8 ms from the four photodiodes surrounding the turned-on LED. While the four LEDs are flashing sequentially within a 200-ms period, a total of 16 bio-optical measurements can be obtained through a time-division multiplexing operation.

The aforementioned sequence allows fully synchronized 16-channel EEG and 16-channel bio-optical measurements to be acquired every 4 ms ($= 250$ SPS) and 200 ms ($= 5$ SPS), respectively. The acquired measurements are then packetized and successively transmitted to the host device via the SPBT3.0 DP2 Bluetooth module (STMicroelectronics, USA) with a header and timing information. The host device decodes the packets of EEG and bio-optical data using MATLAB 2014a (MathWorks, USA). Using the Modified Beer-Lambert Law [37], [38] in the decoding process, the 8-channel fNIRS data, including concentration changes in the oxy- (ΔHbO), deoxy- (ΔHbR), and total hemoglobin (ΔHbT), are also converted from the 16-channel bio-optical data.

The MCU system was programmed to perform the following operations:

- 1) Peripheral initialization—establishment of peripheral interfaces (SPI interface, general purpose input/output ports, and interrupt routine) and setting up registers of all AFE ICs;
- 2) Launching the data-retrieval loop upon detection of the start trigger;
- 3) Acquisition of EEG data from ADS1299, when a DRDY pulse is generated;
- 4) Control of NIR LED emission in accordance with the LED switching schedule and DRDY trigger;
- 5) Acquisition of bio-optical data of the predefined photodiode sets from ADS8688A in accordance with the LED control sequence;
- 6) Packetization of acquired EEG and bio-optical data along with header and timing indication and subsequent

transmission of data packets to the host device via the Bluetooth module;

- 7) Repeating steps 3 through 6 until the stop trigger is detected.

IV. EVALUATION AND EXPERIMENT

A. Evaluation of EEG and fNIRS Acquisition

1) **EEG Phantom Experiment using Dry Electrodes:** The proposed HBM system employs dry electrodes for EEG acquisition instead of the conventional wet electrodes for wide applicability and enhanced usability. Therefore, it is necessary to verify the acquisition capability of the dry electrodes at the level of micro-voltage amplitudes. In the proposed system, the fNIRS and EEG acquisition circuits operate simultaneously. Thus, EEG signal acquisition is subjected to interference from the electrical switching noise generated by the NIR LEDs and this effect must be examined. For this purpose, we devised an EEG phantom experiment.

First, EEG-like voltage signals were generated. Raw EEG data samples of 60-s duration were taken from the C3 channel of a BCI competition 3-IVa dataset (motor imagery task, down-sampled to 250 Hz) [39]. These EEG data samples were then inputted to an arbitrary waveform generator (Keysight 33220A) for reproduction of a EEG voltage waveform. The reproduced voltage waveform was then passed through a voltage divider circuit (of 10000:1 ratio) to create a microvolt-level EEG signal. This voltage waveform was finally fed to the EEG phantom.

Second, an EEG phantom was created using a conductive rubber pad ($10\text{ cm} \times 12\text{ cm} \times 5\text{ mm}$, $100\ \Omega/\text{cm}$) to simulate a real human scalp. An NIR LED unit is placed at the center of the rubber pad. Then, one dry and one wet electrode (with conductive gel) were attached around the LED unit on the rubber pad to emulate the NIR interference during EEG signal measurement. The two electrodes and the NIR LED unit were connected the EEG input port and NIR LED driving port of the HBM, respectively. The EEG reference input of the HBM system was connected to the ground potential of the waveform generator.

Third, the voltage waveform of 60-s duration prepared in the first step was reproduced in the EEG phantom. Measurement samples were recorded at a sampling speed of 250 SPS from the two electrodes during the 60-s period. The two acquired signals were compared with the prepared voltage waveform in terms of correlation coefficients. In offline analysis, three correlation coefficients were calculated and analyzed depending on the NIR LED ON/OFF state. The correlation coefficient between the acquired signal using a dry electrode and the prepared waveform is ρ_D ; the correlation coefficient between the acquired signal using a wet electrode and the prepared waveform is ρ_W ; and the correlation coefficient between two acquired signals obtained using a wet electrode and a dry electrode is ρ_{DW} . To ensure reliability of the analysis, this test was repeated thrice, and the averaged correlation coefficients were compared.

2) Arterial Occlusion Experiment: The hemodynamic response of the proposed system was verified by evaluating the fNIRS responsivity using an arterial occlusion experiment [22], [23]. The experiment was performed using an inflatable arm cuff and a sphygmomanometer. The arm cuff could be shrunk to block arterial blood flow to artificially change the concentration of oxy and deoxy hemoglobin in the bloodstream on the arm. This would enable us to verify the hemodynamic behavior of the proposed system by observing this occlusion through NIRS data acquisition and offline analysis.

For the experiment, NIR LEDs and photodiodes were attached to a subject's arm in the layout shown in Fig. 5. The experiment was carried out for 5 min. The first minute of the experiment was used as the baseline observation before constriction of the cuff. After 1 min, the pressure was increased to 200 mmHg for 6 s and maintained at this level for 2 min, and then, the contraction was released. Through offline analysis, recorded hemodynamic responses were filtered with a 4th order zero-phase Butterworth 0.2-Hz low-pass filter and normalized responsivities for all channel measurements were derived.

B. Human Subject Studies-Alpha Rhythm Detection Test and Mental Arithmetic Experiment

Although the evaluation and verification of the EEG and fNIRS acquisition system were conducted through the EEG phantom and fNIRS responsivity tests, an experiment involving a human subject also needed to be carried out to evaluate the practical applicability in hybrid EEG/fNIRS monitoring. To this end, an alpha rhythm detection test and a mental arithmetic experiment were carried out. The first is a basic level test to determine whether the proposed system is effective for EEG acquisition. The second is a more challenging experiment to establish whether the system can be used to discern the subtle difference in the EEG and fNIRS signal patterns when the brain engages in non-trivial mental activity, i.e., a mathematical *subtraction* operation.

The alpha rhythm is the most well-known EEG feature that can be easily detected when the user closes his or her eyes. When the eyes are closed, the spectral power of the alpha rhythm band (8–15 Hz) is amplified relative to the other spectral ranges. By comparing the spectral power when the eyes are closed and

when they are not, the detection capability of real EEG features can be verified. One subject participated in this test. Ten trials were performed and one trial consisted of maintaining the eye-open state for 12.5 ± 2.5 seconds and the eye-closed state for 10 seconds. In every transition of the command, a beep sound was used to alert the subject to the change of instruction.

The mental arithmetic experiment is designed to examine the functional brain activation that occurs when subjects are required to carry out non-trivial mathematical operations. During a *subtraction* operation, the brain activation can be observed in both EEG and fNIRS signals. In the EEG signals, the activation appears in the form of an event-related desynchronization (ERD) or event-related synchronization (ERS) [40], known as spectral and suppression and enhancement of the measured EEG signals. The activation in the fNIRS signals is also shown as a hemodynamic difference in oxy- and deoxy-hemoglobin concentration changes (ΔHbO , ΔHbR) [41]. We can investigate these distinctive responses through offline analysis, such as time-frequency analysis of the EEG measurements and time-course analysis of the fNIRS measurements.

Including the subject who participated in the alpha rhythm detection experiment, a total of three subjects voluntarily participated in the mental arithmetic experiment. All subjects (three males, average age: 26.3 ± 1.7 years old) were healthy and had no record of neurological and psychiatric disorders. Each subject was given a summary of the experiment and signed a consent form before their participation started.

The subjects were seated on a chair in front of a 24-inch LCD monitor. Prior to the experiment, pilot signal monitoring was performed to check the adhesion state of the probe set and baseline noise characteristics of the acquired EEG signals. The experiment consisted of two sessions, and each session consisted of 10 trials. In a trial, a white fixation cross was displayed while waiting for the next task period in the first 22.5 ± 2.5 s. In this resting state, the subjects were instructed to gaze at the center cross sign and to refrain from any thinking to maintain a low mental load. During the next task period, the subjects were instructed to *cumulatively* subtract a two-digit random prime number (ranging from 10 to 30) from a three-digit random number in the range 500 to 999 for 20 s. For example, the problem of subtracting 13 from 700 is presented to the subject via a computer screen, i.e., “700 – 13.” The subject had to solve this problem by subtraction inside his/her head. Once he/she arrived at the answer to the problem, $687 = 700 - 13$, they were required to memorize it and to continue to subtract another 13 from the answer, i.e., “687 – 13.” This continued until the end of the task period.

EEG measurements were conducted by attaching 16 dry electrodes to the scalp with the fabricated EEGCAP. To observe the task-related activation in the overall brain areas, 16 electrode positions covering the frontal (Fz, F3, F4, Fc1, Fc2, Fc5, and Fc6), motor/temporal (C3 and C4), and parietal (Pz, P3, P4, Cp1, Cp2, Cp5, and Cp6) regions were carefully chosen in accordance with the international 10–20 system. Reference and bias electrodes were also attached to the skin behind the left and right earlobes, respectively, using disposable wet electrodes. The EEGCAP equipped with dry electrodes was fastened to a

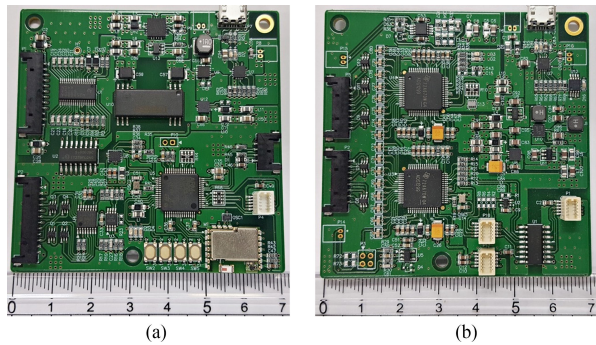


Fig. 7. Images of the (a) main board, and (b) slave board, of the proposed HBM system.

strap on the subject's chest. Two NIR LEDs and six photodiodes were also installed on the forehead using double-sided adhesive tape according to the probe layout in Fig. 5. These installation procedures may take less than 10 minutes, as there is no need for a series of additional preparation processes, such as hair arrangement and scalp abrasion. The EEG and fNIRS measurements acquired by the installed electrodes and photodiodes were simultaneously recorded with an event trigger in real time using MATLAB 2014a.

Offline analysis for the acquired EEG and fNIRS datasets was performed using MATLAB 2014a and EEGLAB toolbox [42]. The EEG datasets were obtained from both the alpha rhythm detection test (one subject participated) and mental arithmetic experiments (three subjects participated). Each EEG dataset was bandpass filtered with a 4th order zero-phase 0.5–40 Hz Butterworth filter. From the filtered dataset, each epoch before and after task onset (−10 to +10 s for the alpha rhythm detection dataset and −15 to +15 s for the mental arithmetic experiment dataset) was extracted based on the recorded event trigger. An EEGLAB built-in function is utilized to investigate ERD/ERS patterns for the time-frequency analysis of the EEG dataset. To visualize the grand-averaged ERD/ERS patterns for each experiment, we averaged the time-frequency decomposition outcomes for all sessions and all subjects who participated. The fNIRS datasets, which comprise the relative concentration changes of oxy-, deoxy- and total hemoglobin (ΔHbO , ΔHbR , and ΔHbT), were only obtained from the mental arithmetic experiments (three subjects participated). A 4th order zero-phase 0.01–0.2 Hz Butterworth bandpass filter was applied to the fNIRS datasets and each epoch was extracted similarly to the EEG pre-processing procedure. Baseline correction of the extracted epoch was performed by subtracting the averaged fNIRS data measured in the resting state between −5 s and 0 s. Identification of the grand-averaged hemodynamic trends during arithmetic operations was also obtained by averaging each of the hemodynamic time courses in the same manner the grand-averaged ERD/ERS patterns were derived.

V. RESULTS

A. System Implementation

Images of the circuit boards of the proposed HBM system for EEG and fNIRS acquisition are shown in Fig. 7. Two

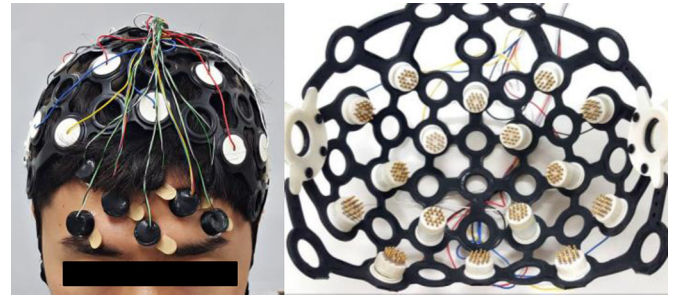


Fig. 8. Image of the complete system comprising the fNIRS probe set and rubber EEGCAP, including 16-channel dry electrodes. The dry electrodes were tightly engaged in the electrode-positioning holes for fixed electrode placement.

TABLE I
CORRELATION COMPARISON FOR ARTIFICIALLY GENERATED EEG RECORDING

NIR LED states	ρ_D	ρ_W	ρ_{DW}
On	0.9422	0.9423	0.9995
Off	0.9433	0.9437	0.9996

four-layered 70 × 70 mm PCBs were fabricated for 16-channel EEG and 8-channel fNIRS acquisition. These boards are connected to each other through the board-to-board connector and are powered by two 2,000 mAh lithium polymer batteries. Sixteen-channel dry electrodes with 18 spring-loaded probes were installed in the EEGCAP, as shown in Fig. 8. Six-channel NIR photodiodes and 2-channel NIR LEDs were also fabricated as depicted in Fig 4(b) and (c). In the experiment involving human subjects, installation of the dry electrodes and the fNIRS probe set was easily accomplished by attaching the set of NIR photodiodes and LED units to the subject's forehead and by requesting the subject to wear the EEGCAP equipped with dry electrodes.

B. Dry-Electrode Evaluation

The correlation coefficients for each electrode comparison set (dry electrode vs. raw signal, wet electrode vs. raw signal, and dry electrode vs. wet electrode) evaluated with the EEG phantom are summarized in Table I. A ρ_{DW} value close to one indicates that the dry and wet electrodes detect almost the same waveform regardless of the activation of the NIR LEDs. This confirms that the dry electrode is capable of obtaining EEG signals without the use of conductive gels and provides almost the same EEG measurement as the wet electrode. Values of ρ_D and ρ_W above 0.9 indicate that the phantom measurements through the dry and wet electrodes are not significantly different from the raw signal data. The slight decrease in the correlation coefficient, compared to ρ_{DW} , is considered to be caused by the error that occurred in the waveform-reduction process using the voltage-divider circuit during artificial EEG generation.

The waveforms recorded by the wet and dry electrodes on the EEG phantom, and the raw EEG signal are shown in Fig. 9(a). The signal recorded at the dry electrode looks like amplified

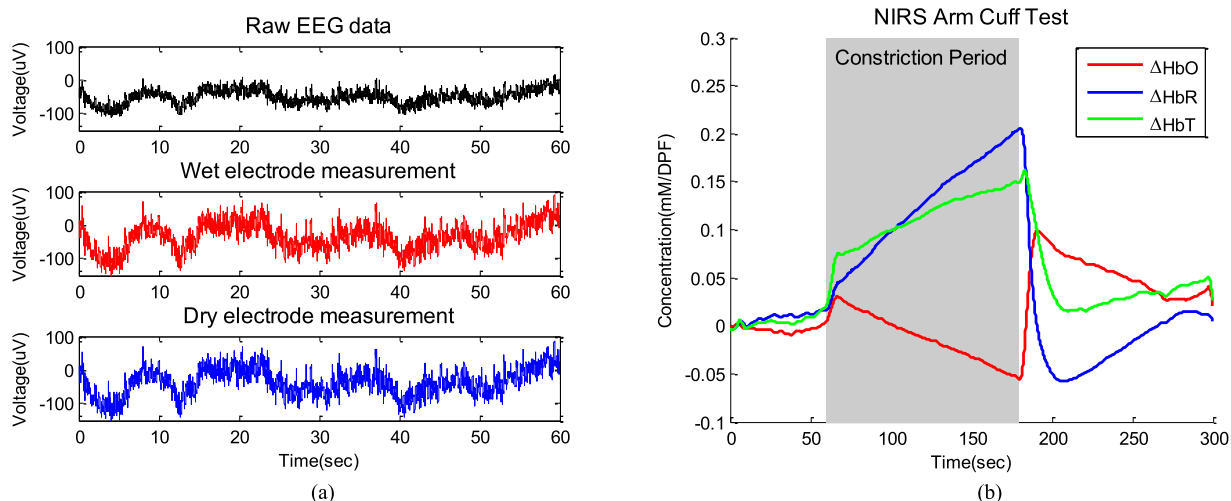


Fig. 9. (a) Comparison of the raw EEG signal and waveforms recorded by the wet and dry electrodes on the EEG phantom, (b) Normalized hemodynamic responses over the eight bio-optical channels with an arterial occlusion experiment.

version of the original signal; however, the overall trend of the waveform is not significantly different according to the correlation coefficient greater than 0.9.

C. fNIRS Response Evaluation

The 8-channel normalized ΔHbO , ΔHbR , and ΔHbT levels were obtained from the offline analysis of the data captured during the arterial occlusion experiment and these results are plotted in Fig. 9(b). All hemodynamic responses converge towards the baseline within ± 0.02 mM / DPF during the first 60 s before contraction of the cuff and increase rapidly over 6 s when the cuff is inflated. When the contraction is complete, the inflowing arterial blood is almost blocked and therefore, the ΔHbO and ΔHbR are linearly diverged until the moment the cuff is released. The slope of the ΔHbO and ΔHbR are $-0.7 \mu\text{M}/\text{DPF}\cdot\text{s}$ and $+1.4 \mu\text{M}/\text{DPF}\cdot\text{s}$, respectively. When the pressure on the cuff is released to allow the arterial blood flow to return, the ΔHbO and ΔHbR dramatically converge and overshooting occurs. After peaking to the opposite overshoot, all hemodynamic responses gradually converge to the steady state. Compared with previous studies [22], [23], in which the same experiment was conducted, the results of this experiment demonstrate that the proposed HBM system is sufficiently responsive to analyze the changes in the hemoglobin concentration.

D. Analysis of Human Subject Studies

The results of the grand-averaged time-frequency analysis results and a comparison of the normalized spectra of the alpha rhythm detection test are depicted in Fig. 10(a) and (c). The vertical dashed lines on the time-frequency analysis plot at 0 seconds denote the onset of the eye-closing task period.

In the alpha rhythm detection test, the event-related synchronization (ERS) pattern evoked by the instruction to close the eyes is clearly indicated with higher spectral power (red zones at Fig. 10(a)) in the alpha rhythm placed in the 8–13 Hz bands compared to the baseline spectral power of -7.5 to -2.5

s. The high spectral power of the beta rhythm in the range of 20–24-Hz at the beginning of the task is considered to be a harmonics related to the high spectral power of the alpha rhythm. The first and second maximum ERS intensities, i.e., 3.74 dB at 11.46 Hz and 2.13 dB at 21.16 Hz, were observed from the dB scale comparison of the normalized spectral graphs at Fig. 10(c). Based on these results, which show that the alpha rhythm associated with closure of the eyes can be detected by using spectral analysis, it is evident that the proposed system can appropriately acquire the general EEG feature signals.

The results of the grand-averaged time-frequency analysis and comparison of the normalized spectra recorded during the mental arithmetic experiments are depicted in Fig. 10(b) and (d). The spectral pattern of the time-frequency analysis was calculated based on the spectral power during the resting state (-15 to -5 s). Compared to the spectral pattern during the task period with those of the alpha rhythm detection test, it is evident that reversed patterns of the spectral perturbation are observed. First and second major event-related desynchronization (ERD) patterns are observed in the alpha rhythm at approximately 10 Hz and in the wide beta rhythm range 18–25 Hz, during the cumulative subtraction task period. The maximum ERD intensity of -2.62 dB at 10.79 Hz in the alpha rhythm range was observed from the dB scale comparison of the normalized spectral graphs in Fig. 10(d). The second highest ERD intensity is -2.10 dB at 19.49 Hz in the beta rhythm range.

The grand-averaged time courses of the concentration changes in oxy-, deoxy- and total hemoglobin (ΔHbO , ΔHbR , and ΔHbT) in the mental arithmetic experiments are plotted in Fig. 11. During the cumulative subtraction task, which is given to the subject to increase the workload level of the brain, we found a clear decreasing trend of ΔHbO . The diminished ΔHbO level is then rapidly restored again to the resting state after the task periods. In contrast, ΔHbR shows a weaker inverse pattern and more delayed response compared to the ΔHbO trend. The lowest ΔHbO is recorded just before the end of the task, whereas the ΔHbR trend continues to increase slightly after the task

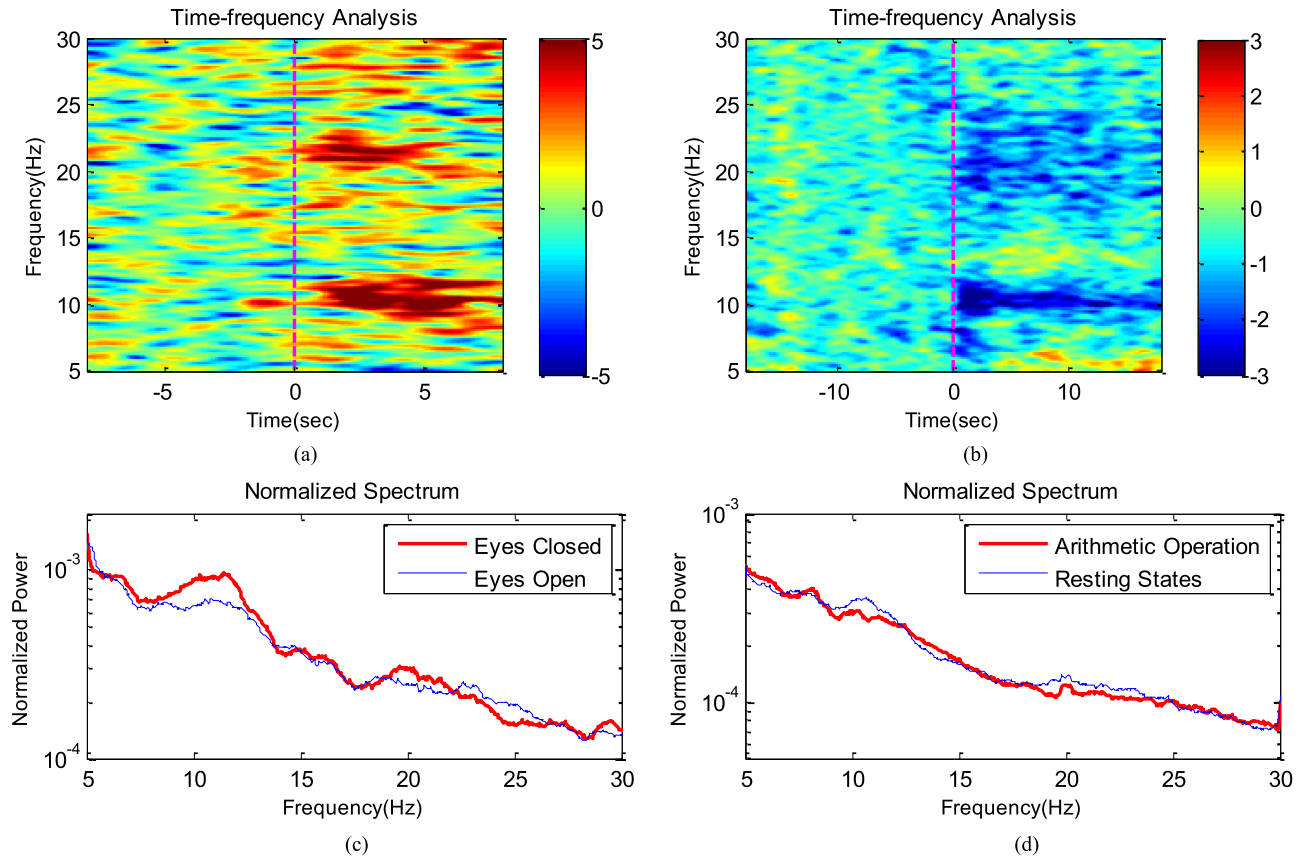


Fig. 10. Results of grand averaged time-frequency analysis (dB scale) for the alpha rhythm detection test (a) and mental arithmetic experiments (b). Vertical dashed lines indicate task onset. Red and blue zones mean the time and frequency ranges associated with high event-related synchronization (ERS) and desynchronization (ERD). Spectral comparisons (c) and (d) are normalized spectra for each task states ((c) eye open states vs. eye closed states, (d) arithmetic operating states vs. resting states).

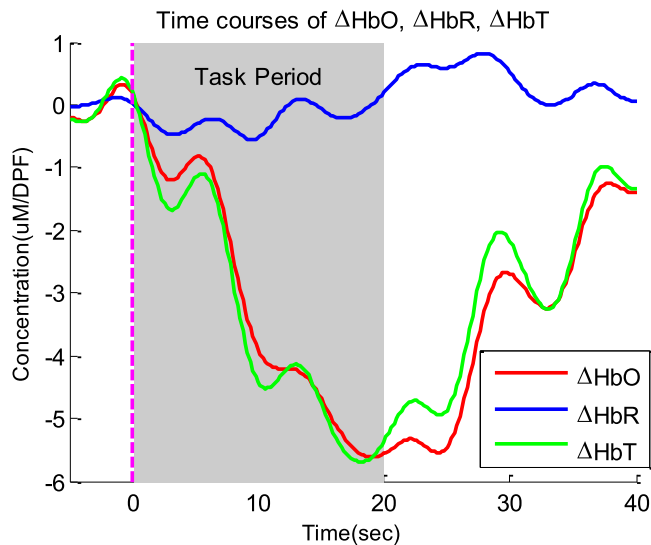


Fig. 11. Grand-averaged time courses of concentration changes in oxy-, deoxy- and total hemoglobin (ΔHbO , ΔHbR , and ΔHbT) for mental arithmetic experiments.

period. This ΔHbR trend begins to decrease belatedly at 8 s after the end of the task. These analysis results show that the ΔHbO pattern much more closely reflects the mental workload

level than the weaker ΔHbR response and the ΔHbT pattern also follows the more dominant ΔHbO trend.

The EEG and fNIRS responses in the mental arithmetic experiments provided the brain activation responses such as the ERD pattern on the alpha and beta rhythm bands and the decreasing trend of the ΔHbO response. These results were compared with those obtained in the previous study [43], in which similar experiments were conducted using commercial equipment. Based on our studies with human subjects, we can conclude that the proposed HBM system has sufficient capabilities to simultaneously monitor EEG and fNIRS signals.

VI. DISCUSSION

The system specifications and key differences compared with the previous studies are summarized in Table II.

[Electrodes] Compared to all previous studies, the proposed system is the first to apply the spring-loaded dry electrodes. More than one hour of continuous EEG monitoring using the conventional wet electrodes is difficult because the conductive gel needs to be replenished every time it becomes dry. Because the dry electrodes enable gel-less EEG acquisition, the quality of the measurement is not degraded and longer experimentation is possible for daily-life monitoring. In addition, it is easy to

TABLE II
COMPARISON OF SYSTEM SPECIFICATIONS AND CONTRIBUTIONS WITH PREVIOUS STUDIES

Comparison category		[21], [22]	[23]	[24]	Proposed
System Specification	# of EEG electrodes	8	16	4	16
	# of LED/PD	8/8	32/4	2/2	8/8
	EEG resolution, ADC architecture	16 bit, Undefined	16 bit, SAR	24 bit, Δ - Σ	24 bit, Δ - Σ
	fNIRS resolution, ADC architecture,	16 bit, Undefined	16 bit, Δ - Σ	24 bit, Δ - Σ	16 bit, SAR
	Volume efficiency	106.6 cm ³ /ch	1.4 cm ³ /ch	1.7 cm ³ /ch	2.0 cm ³ /ch
	Power efficiency, operation hour with 3.7 V 1 Ah battery	150 mW/ch 1.5 h	20 mW/ch 9.25 h	61.6 mW/ch 10 h	18.8 mW/ch 8.2 h
Dry electrode-based EEG acquisition		No	No	Not yet	Yes
Fully isolated circuit design		No	No	No	Yes
Linear regulator-based low-noise power supply		No	No	Yes	Yes
Customizable EEG electrode-positioning structure		Undefined	No	No	Yes

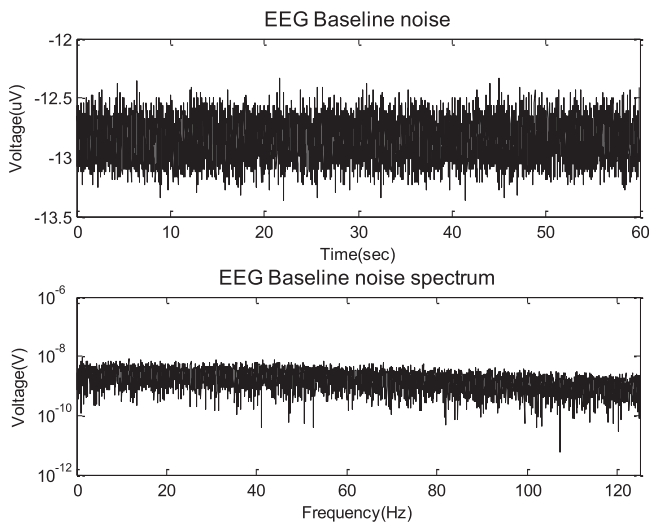


Fig. 12. EEG baseline noise measurements and their spectrum, under the NIR LED activated condition.

install without irritation, a shortened system setup time, and reduced complexity of the experiment.

[Isolated and low-noise circuit design] The implementation of an isolated circuit design is also a first attempt compared to previous studies. Owing to the complete separation of the EEG, fNIRS, and control circuitries with a linear regulator-based low-noise power supply, the proposed system is able to achieve excellent low-noise characteristics for EEG acquisition. During the EEG phantom test, the input-referred noise of the EEG acquisition circuit was evaluated using the built-in input-shorted function of an ADS1299 and its results are shown in Fig. 12. Even with the LED flashing condition, an input-referred noise of $0.141 \mu\text{V}_{\text{RMS}}$ and $1.066 \mu\text{V}_{\text{pp}}$ was measured and no crosstalk component was observed in the spectrum. These results verified

that the proposed system closely achieves the low-noise characteristics of $0.14 \mu\text{V}_{\text{RMS}}$ and $0.98 \mu\text{V}_{\text{pp}}$ (at a sampling rate of 250 SPS and a 24 PGA gain) as specified in the ADS1299 datasheet [29].

[Frontend design] Compared to previous studies on system specifications, the proposed system employs two different kinds of architecture-optimized AFE ICs to simultaneously provide superior EEG resolution and delay-less bio-optical measurement. Because high resolution and continuous sampling are required for EEG measurement, the conversion delay can be considered negligible and the 24-bit Δ - Σ ADC is ideal for use. However, in the case of bio-optical measurements, on-time data acquisition is more important than resolution performance because the sampling is required only for specific predefined time periods along the preprogrammed LED emission schedule. The Δ - Σ ADC-based ADS1299 has a conversion latency of 16 ms at a 250-SPS sampling rate, whereas the SAR ADC-based ADS8688A always maintains a data conversion time of up to $0.85 \mu\text{s}$, regardless of the sampling rate setting. Therefore, this instantaneous sampling characteristic prevents sampling errors in the bio-optical measurements caused by the phase transition of LED activation and ensures system reliability.

[System specifications] The positioning-customizable 16-channel EEG electrodes and 8-channel photodiode detectors indicate that the proposed system is ready for clinical applications for which sufficient spatial resolution is required. However, the estimated volume efficiency (system volume per number of EEG and PD channels) has been slightly reduced due to the implementation of advanced design techniques, such as isolation design and low-noise power supply. Nevertheless, the system size is such that it is still portable ($7 \times 7 \times 1 \text{ cm}^3$) and the power efficiency (power consumption per number of EEG and PD channels) is considerably improved, thus the operation time can be extended to more than 8 hours with a 1-Ah lithium polymer battery. This extended operation time adds the benefit

of a spring-loaded dry electrode that maintains good scalp contact without a conductive gel, facilitating hybrid brain monitoring in out-of-lab situations.

[Limitations and future development] One of the limitations is that it is difficult to obtain fNIRS measurements in various brain areas because the NIRS probes can only be attached to the hairless scalp. Overcoming this challenge necessitates the design of a probe structure that can be adhered to the scalp by applying pressure with a stretchable structure such as the spring-loaded structure of a dry electrode.

The achievement of stable EEG quality in an actual out-of-lab situation requires motion artifacts to be removed from EEG measurements. Therefore, a movement monitoring function is required, and it can be implemented by integrating a MEMS-based inertial sensor. A continuous impedance check function is also required to monitor the adhesion of the electrode in real time, because the adhesion pressure of the electrode has a significant effect on the quality of the acquired EEG signal. This function can be implemented by utilizing the built-in lead-off detection function with the ADS1299.

VII. CONCLUSION

In this study, a hybrid brain monitoring system for simultaneous acquisition of 16-channel EEG and 8-channel fNIRS has been proposed. A single low-power microcontroller unit synchronously controls two kinds of architecture-optimized AFE ICs to achieve fully synchronized data acquisition. Employing Δ - Σ ADC-based ADS1299 and SAR ADC-based ADS8688A simultaneously, the proposed system achieves 24-bit EEG resolution and delay-less ($<0.85 \mu\text{s}$) reliable fNIRS measurements. A fully isolated design, which completely separates the ground plane of each circuit section by using digital isolators and an isolated DC-DC converter, physically blocks inter-circuit interference. The isolated design applied with a linear regulator-based low-noise power supply improves system reliability and noise immunity for EEG/fNIRS measurements. Moreover, the use of spring-loaded dry electrodes and EEGCAP shortens system-wearing time and continuously provides stable EEG quality. It will allow longer experiments for out-of-lab applications. The acquisition of EEG and fNIRS measurements was evaluated by conducting an EEG phantom test using artificially generated EEG signals and an arterial occlusion experiment. Additionally, an alpha rhythm detection test and mental arithmetic experiments were performed to assess the practical capabilities of the proposed system for human subject studies. The grand-averaged results of the time-frequency analysis for EEG measurements and time courses for NIRS measurements verified that the proposed HBM systems are suitable for use in real BCI applications.

REFERENCES

- [1] J. R. Wolpaw *et al.*, "Brain-computer interfaces for communication and control," *Clin. Neurophysiol.*, vol. 113, no. 6, pp. 767–791, 2002.
- [2] L. F. Nicolas-Alonso and J. Gomez-Gil, "Brain computer interfaces, a review," *Sensors (Basel)*, vol. 12, no. 2, pp. 1211–1279, Jan. 2012.
- [3] J. D. R. Millán *et al.*, "Combining brain–computer interfaces and assistive technologies: State-of-the-art and challenges," *Frontiers Neurosci.*, vol. 4, Sep. 2010, Art. no. 161.
- [4] M. D. Murphy *et al.*, "Current challenges facing the translation of brain computer interfaces from preclinical trials to use in human patients," *Frontiers Cellular Neurosci.*, vol. 9, Jan. 2016, Art. no. 497.
- [5] C. Vidaurre and B. Blankertz, "Towards a cure for BCI illiteracy," *Brain Topography*, vol. 23, no. 2, pp. 194–198, 2010.
- [6] G. Pfurtscheller *et al.*, "The hybrid BCI," *Frontiers Neurosci.*, vol. 4, Apr. 2010, Art. no. 42.
- [7] N. Weiskopf, "Real-time fMRI and its application to neurofeedback," *NeuroImage*, vol. 62, no. 2, pp. 682–692, Aug. 2012.
- [8] T. Nguyen *et al.*, "Utilization of a combined EEG/fNIRS system to predict driver drowsiness," *Sci. Rep.*, vol. 7, Mar. 2017, Art. no. 43933.
- [9] A. Machado *et al.*, "Detection of hemodynamic responses to epileptic activity using simultaneous Electro-Encephalography (EEG)/Near Infra Red Spectroscopy (NIRS) acquisitions," *NeuroImage*, vol. 56, no. 1, pp. 114–125, May 2011.
- [10] N. Naseer and K.-S. Hong, "fNIRS-based brain-computer interfaces: A review," *Frontiers Human Neurosci.*, vol. 9, Jan. 2015, Art. no. 3.
- [11] S. Amiri *et al.*, "A review of hybrid brain-computer interface systems," *Adv. Human-Comput. Interaction*, vol. 2013, 2013, Art. no. e187024.
- [12] S. Fazli *et al.*, "Enhanced performance by a hybrid NIRS–EEG brain computer interface," *NeuroImage*, vol. 59, no. 1, pp. 519–529, Jan. 2012.
- [13] A. P. Buccino *et al.*, "Hybrid EEG-fNIRS asynchronous brain-computer interface for multiple motor tasks," *PLOS ONE*, vol. 11, no. 1, 2016, Art. no. e0146610.
- [14] S. Ge *et al.*, "A brain-computer interface based on a few-channel EEG-fNIRS bimodal system," *IEEE Access*, vol. 5, pp. 208–218, 2017.
- [15] R. Li *et al.*, "Enhancing performance of a hybrid EEG-fNIRS system using channel selection and early temporal features," *Frontiers Human Neurosci.*, vol. 11, Sep. 2017, Art. no. 462.
- [16] A. M. Chiarelli *et al.*, "Deep learning for hybrid EEG-fNIRS brain-computer interface: application to motor imagery classification," *J. Neural Eng.*, vol. 15, no. 3, 2018, Art. no. 036028.
- [17] Y. Tomita *et al.*, "Bimodal BCI using simultaneously NIRS and EEG," *IEEE Trans. Biomed. Eng.*, vol. 61, no. 4, pp. 1274–1284, Apr. 2014.
- [18] M. J. Khan *et al.*, "Decoding of four movement directions using hybrid NIRS-EEG brain-computer interface," *Frontiers Human Neurosci.*, vol. 8, Apr. 2014, Art. no. 244.
- [19] H. Aghajani *et al.*, "Measuring mental workload with EEG+fNIRS," *Frontiers Human Neurosci.*, vol. 11, Jul. 2017, Art. no. 359.
- [20] R. J. Cooper *et al.*, "Design and evaluation of a probe for simultaneous EEG and near-infrared imaging of cortical activation," *Phys. Med. Biol.*, vol. 54, no. 7, pp. 2093–2102, 2009.
- [21] E. Lareau *et al.*, "Multichannel wearable system dedicated for simultaneous electroencephalography /near-infrared spectroscopy real-time data acquisitions," *J. Biomed. Opt.*, vol. 16, no. 9, 2011, Art. no. 096014.
- [22] M. Sawan *et al.*, "Wireless recording systems: From noninvasive EEG-NIRS to invasive EEG devices," *IEEE Trans. Biomed. Circuits Syst.*, vol. 7, no. 2, pp. 186–195, Apr. 2013.
- [23] J. Safaie *et al.*, "Toward a fully integrated wireless wearable EEG-NIRS bimodal acquisition system," *J. Neural Eng.*, vol. 10, no. 5, 2013, Art. no. 056001.
- [24] A. von Lüthmann *et al.*, "M3BA: A mobile, modular, multimodal biosignal acquisition architecture for miniaturized EEG-NIRS-based hybrid BCI and monitoring," *IEEE Trans. Biomed. Eng.*, vol. 64, no. 6, pp. 1199–1210, Jun. 2017.
- [25] S. Lee *et al.*, "Dry electrode design and performance evaluation for EEG based BCI systems," in *Proc. Int. Winter Workshop Brain-Comput. Interface*, 2013, pp. 52–53.
- [26] L.-D. Liao *et al.*, "Design, fabrication and experimental validation of a novel dry-contact sensor for measuring electroencephalography signals without skin preparation," *Sensors*, vol. 11, no. 6, pp. 5819–5834, May 2011.
- [27] Y. M. Chi *et al.*, "Dry-contact and noncontact biopotential electrodes: Methodological review," *IEEE Rev. Biomed. Eng.*, vol. 3, pp. 106–119, Oct. 2010.
- [28] S. Karthik and B. Mark, "Analog front-end design for ECG systems using delta-sigma ADCs," Texas Instrum., Dallas, TX, USA, Appl. Rep. SBAA160A, Mar. 2009.
- [29] ADS1299 Datasheet. Texas Instrum., Dallas, TX, USA, Jul. 2012.
- [30] ADS8688 Datasheet. Texas Instrum., Dallas, TX, USA, Jul. 2015.
- [31] W. Kester and Analog Devices, inc, Eds., *Data Conversion Handbook*. Amsterdam, The Netherlands: Elsevier, 2005.

- [32] B. C. Baker, "Conversion latency in delta-sigma converters," Texas Instrum., Dallas, TX, USA, 2007.
- [33] S. Pithadia and S. More, "Grounding in mixed-signal systems demystified, Part 1," Texas Instrum., Dallas, TX, USA, 2013.
- [34] W. Alexander and P. Alexander, "High-speed layout guidelines," Texas Instrum., Dallas, TX, USA, Appl. Rep. SCAA082, Nov. 2006.
- [35] H. Zumbahlen and Analog Devices, inc, Eds., *Linear Circuit Design Handbook*. Amsterdam, The Netherlands: Elsevier, 2008.
- [36] G. Strangman *et al.*, "Non-invasive neuroimaging using near-infrared light," *Biol. Psychiatry*, vol. 52, no. 7, pp. 679–693, Oct. 2002.
- [37] J. G. Kim and H. Liu, "Variation of haemoglobin extinction coefficients can cause errors in the determination of haemoglobin concentration measured by near-infrared spectroscopy," *Phys. Med. Biol.*, vol. 52, no. 20, pp. 6295–6322, 2007.
- [38] L. Kocsis *et al.*, "The modified beer–Lambert law revisited," *Phys. Med. Biol.*, vol. 51, no. 5, p. N91–N98, 2006.
- [39] B. Blankertz *et al.*, "The BCI competition III: Validating alternative approaches to actual BCI problems," *IEEE Trans. Neural Syst. Rehabil. Eng.*, vol. 14, no. 2, pp. 153–159, Jun. 2006.
- [40] G. Pfurtscheller and F. H. Lopes da Silva, "Event-related EEG/MEG synchronization and desynchronization: Basic principles," *Clin. Neurophysiol.*, vol. 110, no. 11, pp. 1842–1857, Nov. 1999.
- [41] G. Pfurtscheller *et al.*, "Focal frontal (de)oxyhemoglobin responses during simple arithmetic," *Int. J. Psychophysiol.*, vol. 76, no. 3, pp. 186–192, Jun. 2010.
- [42] A. Delorme and S. Makeig, "EEGLAB: An open source toolbox for analysis of single-trial EEG dynamics including independent component analysis," *J. Neurosci. Methods*, vol. 134, no. 1, pp. 9–21, Mar. 2004.
- [43] J. Shin *et al.*, "Evaluation of a compact hybrid brain-computer interface system," *BioMed. Res. Int.*, vol. 2017, 2017, Art. no e6820482.